Journal Pre-proof

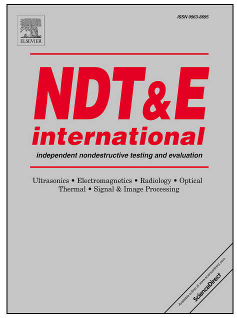

Quantification of porosity in composite plates using planar X-ray phase contrast imaging

D. Shoukroun, L. Massimi, M. Endrizzi, A. Nesbitt, D. Bate, P. Fromme, A. Olivo

PII: S0963-8695(23)00150-0

DOI: https://doi.org/10.1016/j.ndteint.2023.102935

Reference: JNDT 102935

To appear in: *NDT and E International*

Received Date: 15 December 2021

Revised Date: 7 November 2022

Accepted Date: 6 August 2023

Quantification of Porosity in Composite Plates using Planar X-ray Phase Contrast Imaging

D. Shoukroun[1,2], L. Massimi[1], M. Endrizzi[1], A. Nesbitt[3], D. Bate[4], P. Fromme[2], A. Olivo[1]

[1] Department of Medical Physics and Biomedical Engineering, University College London, WC1E 6BT, UK

[2] Department of Mechanical Engineering, University College London, WC1E 6BT, UK

[3] Department of Materials, University of Manchester, M13 9PL, UK

[4] Nikon, X-Tek Systems Ltd., Tring, Hertfordshire, HP23 4JX, UK

Contact Author: D. Shoukroun, dana.shoukroun.17@ucl.ac.uk

Abstract

The application of planar Edge-Illumination X-ray Phase-Contrast imaging (EI-XPCi) for the non-destructive quantification of porosity in carbon fiber reinforced polymer (CFRP) specimens, a significant concern in aerospace applications, was investigated. The method enables fast, planar (2D) scans providing access to large samples. A set of woven CFRP plates with porosity content ranging from 0.7% to 10.7% was examined. In addition to standard X-ray attenuation, EI-XPCi provides differential phase and dark-field signals, sensitive to inhomogeneities and interfaces at scales above and below the system spatial resolution, respectively. The correlation with the porosity content from matrix digestion obtained from the dark-field signal was comparable to that from ultrasonic attenuation. The novel analysis of the standard deviation of differential phase (STDP), sensitive to inhomogeneities above the system resolution (approximately 12 μm), resulted in a very high correlation ($R^2 = 0.995$) with the matrix digestion porosity content, outperforming ultrasonic attenuation measurements.

Keywords: Composites, CFRP, Porosity, Voids, Radiography, XPCi, Ultrasound

1. Introduction

Porosity and voids are a known problem for carbon fiber reinforced polymer (CFRP) structures that occurs during the manufacturing process [1]. Most non-destructive evaluation (NDE) techniques concentrate on the detection and quantification of porosities in the 1-5% range, with porosity levels above 2% typically considered not acceptable by the aerospace industry [2, 3]. CFRP porosity mainly affects mechanical properties, and studies have investigated void formation and distribution in composite samples, for different layups, processing parameters, and manufacturing techniques [4]. Accurate knowledge of void size, shape, and location is required for stress analysis to evaluate the influence on mechanical properties [5]. Matrix (acid) digestion is one of the commonly employed methods to evaluate porosity in composite plates [5], specified in relevant standards [6]. However, it is destructive, and its accuracy depends on accurate knowledge of the properties of the composite constituents and the employed method [5]. The most common NDE methods include X-ray computed tomography (CT) [7-9] and ultrasonic testing [10-12]. X-ray CT imaging offers high resolution and a reliable characterization of the pore size and shape distribution, but it is time consuming and has severe limitations on the sample size to achieve the required resolution. Ultrasonic attenuation measurement is a practical and cost-effective technique with approximately linear correlation to porosity content, but has lower resolution [2]. Ultrasonic C-scans allow the localization and sizing of larger voids, depending on the employed frequency and thus resolution [13]. Active infrared thermography has been shown to similarly allow for the nondestructive localization and sizing of voids above 0.2 mm size in plate specimens [14]. The accuracy and repeatability of the different destructive and nondestructive methods has been investigated and found to be approximately 0.5 percentage points for both matrix digestion and ultrasound, with higher accuracy and repeatability achieved for X-ray CT measurements, depending on the resolution and thresholding technique [5, 7]. Matrix digestion is widely used as the destructive reference method and was shown to have very strong correlation against X-ray CT porosity data [7].

X-ray phase contrast imaging (XPCi) offers a solution for cases where conventional radiography yields low contrast and cannot detect the features of interest. While conventional radiography relies on features having sufficiently different levels of X-ray attenuation, XPCi uses the real part of the refractive index, which is larger than the imaginary part driving the attenuation effects, and is sensitive to phase effects induced by inhomogeneities, thus providing higher contrast [15, 16]. Various XPCi approaches exist, including Talbot-Lau interferometry [17] and free space propagation [18]. Edge Illumination XPCi (EI-XPCi) relies on the refraction of X-rays at the interfaces of inhomogeneities and translates these into a variation of detected intensity using a set of coded aperture masks. With the acquisition of at least three images for different relative mask positions, EI-XPCi allows for the retrieval of conventional attenuation, differential phase, and dark-field images [19]. The differential phase signal corresponds to the angle by which X-rays are refracted by the sample, most pronounced at interfaces. The dark-field signal corresponds to the ultra-small-angle scattering of X-rays due to sample inhomogeneities at the sub-pixel scale, allowing detection of the presence of micro-features smaller than the system resolution without additional adjustments to the experimental setup [20]. This relative simplicity of the setup makes EI-XPCi easily scalable to larger field of views, while enabling relatively fast scans. Using scan-based acquisition systems, samples up to 200 x 500 mm^2 have been imaged [21], which however is not the ultimate limit. EI-XPCi is robust against energy variations and environmental vibrations, and can be used using a polychromatic beam produced by a conventional X-ray source [16, 22].

EI-XPCi was previously used for damage detection in composites, and compared to immersion ultrasonic imaging [23, 24]. This demonstrated the complementarity of the differential phase and dark-field signals to the conventional attenuation signal. The signals have sensitivity to different types of defects, allowing better visualization of the extent of the damage by using the sub-pixel sensitivity of the dark-field signal [23]. XPCi was previously used both for the detection and quantification of porosity in aluminum welds using Talbot-Lau interferometry dark-field CT [25]. The same technique was used to perform CT scans on carbon and glass fiber reinforced composite plates, investigating all three XPCi signals [26]. Overall, these studies show that the phase-based X-ray signals allow for a better detection of inhomogeneities such as pores than can be obtained with conventional radiography. However, all the investigations reported above used XPCi CT imaging, and the option to detect and quantify porosity with planar (2D) XPCi was not explored, which is much faster than CT, removes limitations on sample size [21], and is compatible with online inspection.

In this investigation, the differential phase and dark-field signals were used for the quantification of porosity content using planar EI-XPCi in cross-ply, woven fiber-reinforced composite plates with porosity content varying from 0.7% to 10.7%. The three EI-XPCi signals were compared to ultrasonic immersion through transmission absorption measurements and matrix digestion, the standard industry methods for non-destructive and destructive porosity content evaluation, respectively. This study introduces the use of the standard deviation of the differential phase (STDP) as a means to measure and quantify the variation in the distribution of inhomogeneity in the sample on a scale equal to or above the system resolution and demonstrates this can produce a very high correlation with the porosity content determined by matrix digestion. This complements the results from the dark-field signal, which is sensitive to sub-resolution features.

2. Experimental Methods

Nine CFRP specimens were manufactured with varying degrees of porosity, ranging from 0.7% to 10.7%, using ten 300µm thick plies of M21 epoxy-carbon woven fabric cross-ply pre-preg (Hexcel), with an average plate thickness of 3.0±0.2mm. The standard autoclave cure followed the recommendations for M21 pre-pregs [27] (pressurized at 7bar, heated at 2ºC/min, cure dwell at 180ºC for 120 min, cooled at 5ºC/min, depressurized when temperature is below 60ºC, under 100% vacuum for the total duration of the cure). Different parameters of the cure cycle were varied to obtain specimens with a range of porosities, including varying the debulk duration, edge breathing, autoclave pressure, heating rate, and intermediate dwell. Large panels (160mm by 240mm) were manufactured, and the investigated 100mm by 50mm specimens extracted. One of the specimens (1.5% porosity) was extracted from a smaller panel with dimensions 120 mm by 160 mm. Three smaller samples (20mm by 10mm) were extracted from each large panel adjacent to the extracted specimen (to ensure the main specimens remain available for additional measurements) and used for the determination of porosity content by matrix digestion (ASTM D3171 Procedure B, BS ISO 14127:2008) [28], using nominal densities of 1.78g/cm^3 for the fibers and 1.28g/cm^3 for the matrix. The calculated porosity values (0.7%, 0.9%, 0.9% 1.3%, 1.5%, 3.9%, 5.9%, 6.6%, 10.7%) were used as comparison values in this investigation. Data on pore size distribution was not available, but changes of pore size and shape due to the different ways in which cure parameters were varied should be expected.

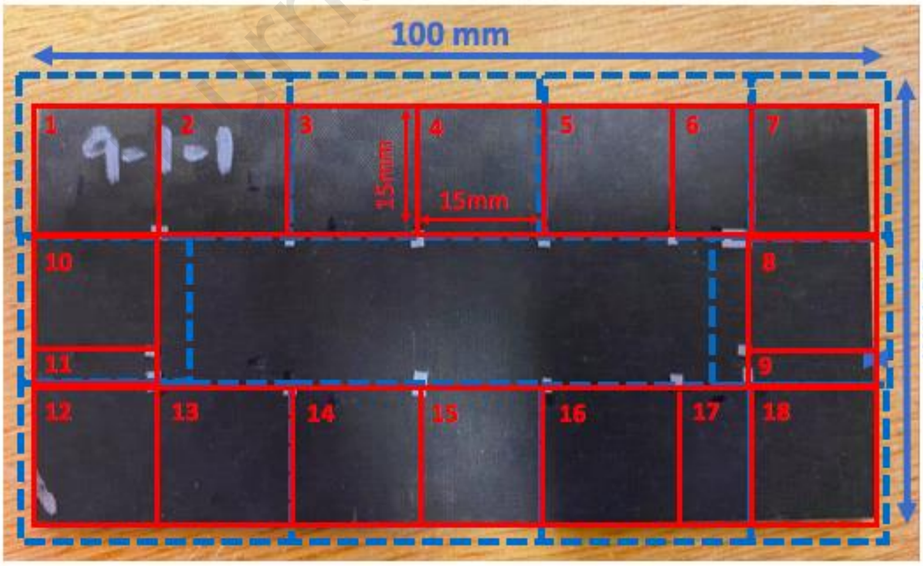

Figure 1: Photograph of one of the 100mm by 50mm porosity plate specimens with the 10 X-ray image acquisition areas and the corresponding 18 ROIs highlighted by dashed blue and solid red lines, respectively. Small reflective tape strips markers for ROI boundaries are visible.

Due to the limited field of view of the X-ray system available for this experiment (20mm by 30mm) and the requirement to include a background area (i.e., keep the edge of the plate in the field of view) for image normalization, the plates were imaged in 10 separate acquisitions, which covered 75% of the outer plate area marked in Fig. 1. The central part of the samples could not be scanned with background area for normalization, and as a result was left out. 18 Regions of Interest (ROIs) were located around the edges of the plates, and identified using reflective tape markers, visible in both ultrasonic imaging and XPCi (13 ROIs of 15 mm by 15 mm, 2 ROIs of 10 mm by 15 mm and 2 ROIs of 5 mm by 15 mm due to size of sample).

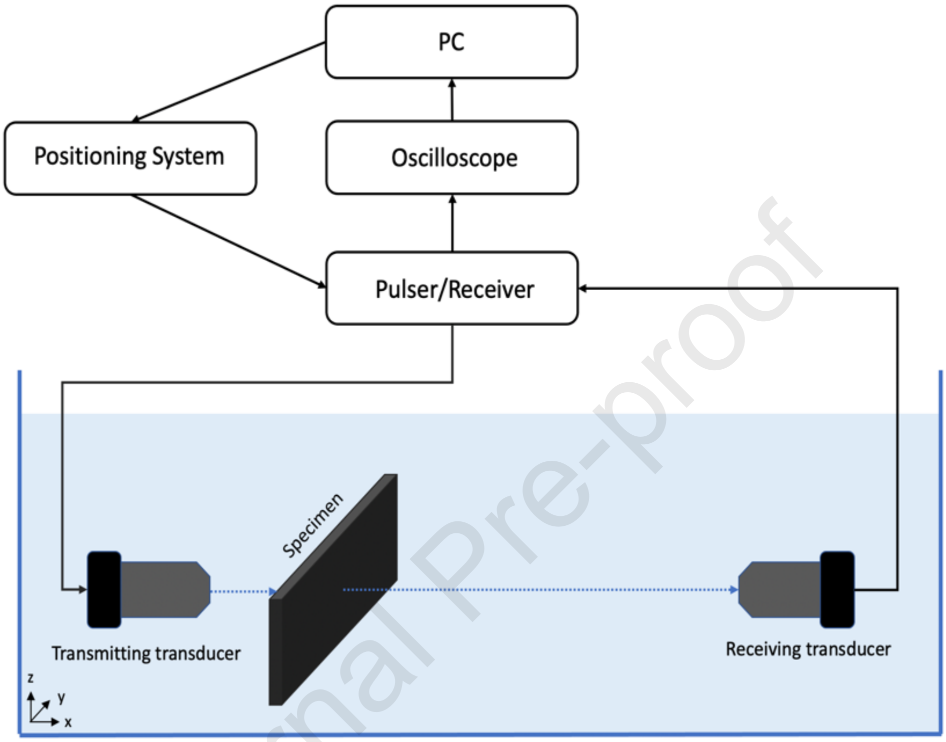

Figure 2: Ultrasonic immersion single through transmission experimental set-up, using two 5MHz transducers for attenuation measurements of the porosity specimens.

The porosity specimens were first analyzed using ultrasonic through transmission C-scans [29]. Two focussed transducers, both with 5 MHz center frequency, were placed on either side on the specimen immersed in water, as shown in Fig. 2. The emitting transducer (Olympus XL50-5-P3) had a nominal diameter of ½ inch (13mm) and a focal length of 19mm. The focal spot diameter was calculated to be 650µm for a wavelength of 300µm. The transducer was excited by the high voltage pulse created by the pulser/receiver (Panametrics 5601T), with the ultrasonic wave propagating through the water and the sample placed at the focal spot. The transmitted signal was captured by the receiving transducer (Ultran U8420169), which had a nominal diameter of ½ inch (13mm), a focal length of 76mm and focal spot of 2.6mm. The receiving transducer was connected to the pulser/receiver, and the received signal was recorded using a digital storage oscilloscope (LeCroy 9304). Each scan consisted of 221 by 121, 500µm steps, which required approximately 8 hours to cover the full sample. The full A-scan signals transmitted through the sample were saved for each scan point and the signal attenuation calculated by comparing the maximum amplitude of the signal transmitted through the water (V_{water}) and through the plate (V_{sample}):

$$\Delta I(dB) = 20\ \log \frac{V_{water}}{V_{sample}}$$

where ΔI is the ultrasonic signal attenuation, measured in decibels (dB). C-scans of the signal attenuation were generated for all plates, and the ultrasonic attenuation values averaged for each specimen to allow comparison with the matrix digestion values.

Planar (2D) X-ray scans of all samples were performed using a laboratory EI-XPCi system [30]. The setup included a Rigaku MicroMax 007 HF rotating anode molybdenum X-ray source with a 70μm focal spot, operated at 40kVp and 20mA. These parameters were chosen as they gave the best trade-off between flux and sensitivity for this investigation [30]. The detector used was a Hamamatsu C9732DK flat panel CMOS detector with a 50μm by 50μm pixel size. The source to detector distance, Z_{SD}, was 0.85m, and the sample stage was positioned 0.7m away from the source. Two coded aperture masks are employed by an EI system, with the first ("sample") mask placed upstream of the sample, and the second ("detector") mask placed in front of the detector, as shown in Fig. 3. The optimal relative positioning of source, masks, sample, and detector was determined previously based on simulations and experimental validation [31].

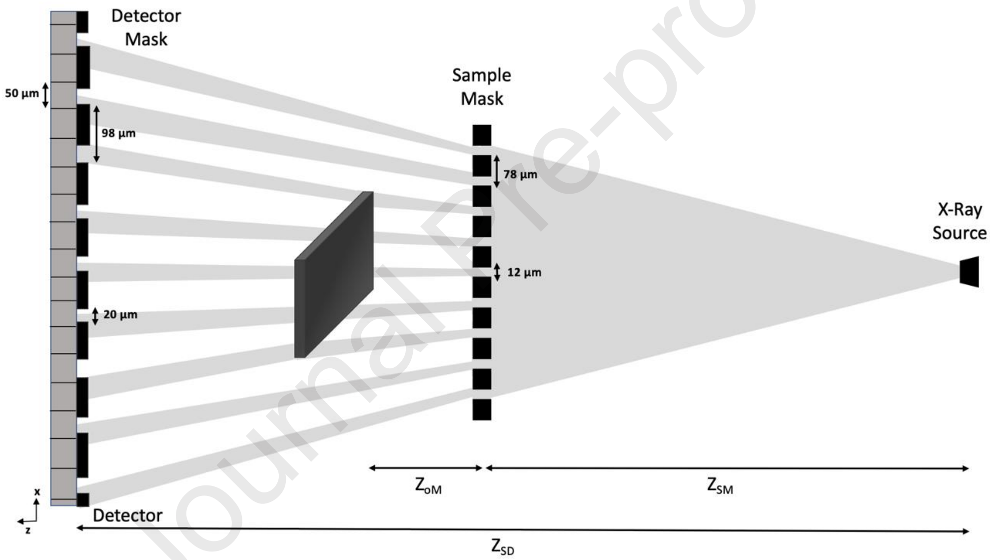

Figure 3: Top-view schematic of the Edge Illumination XPCi experimental setup using a skipped masks aperture system.

The sample and the sample mask were mounted on a series of motors, giving control over the orientation and positioning of the setup components. The sample mask was mounted on a Newport M-ILS150 motor that allows translation along the x-axis with a precision of 0.1μm, a Newport MFA-CC for translation along the z-axis, and a Kohzu cradle SA04B-RM for rotation about the x- and z-axes, with a precision of 0.0014˚. This allowed the alignment of the sample mask apertures with the detector pixel columns and detector mask apertures, and to acquire images with different sample mask positions relative to the detector mask [32]. The sample orientation was kept constant throughout the scanning of all 18 ROIs and for all nine plates, to ensure the same fiber orientation for all scans. The masks were fabricated by MicroWorks to the authors' design by electroplating a layer of gold on a patterned graphite substrate. Apertures consist of equally spaced, narrow slits extending over the entire vertical (y with respect to Fig. 3) dimension of the masks, bar some interruptions introduced at regular intervals to ensure a better adhesion between the gold and substrate. The sample mask, with an aperture size of 12μm, a period of 78μm and positioned 0.65m away from the source (Z_{SM}), splits the incoming divergent beam into an

array of small beamlets. The detector mask had an aperture of 20µm and a period of 98µm to account for beam widening. Both masks were "skipped" masks [33], meaning that every other pixel column was covered by the detector mask (see Fig. 3); this reduces the effects of crosstalk between neighboring pixels in the detector and obtains an aperture limited spatial resolution when combined with dithering acquisition [34]. The overall system magnification was 1.25. The resulting system was only sensitive to phase effects in the x-direction. For radiation safety, the described system is located inside a shielded and interlocked room. Other system prototypes have been developed inside portable shielded cabinets. These typically feature larger sample masks allowing for extended fields of view (e.g., 90 x 90 mm^2 [30]).
The acquisition procedure included collecting a series of flat field images at a range of positions on the "illumination curve" (IC). The IC is the bell-shaped curve obtained by shifting the sample mask along the x-direction while keeping the detector and detector mask fixed, and recording the beam intensity at every position [22]. 19 relative sample mask positions were acquired, with one point at the "top" of the IC where the two masks are perfectly aligned, and 9 additional points taken symmetrically on each side by translating the sample mask position in steps of 4µm. All images were acquired with an exposure time of 6s, resulting in an overall total acquisition time of about 1 hour. Frames at the same 19 IC positions, with the same exposure time, are then acquired after the sample has been introduced. In order to increase the resolution, the samples were dithered, i.e., repositioned along the x-direction at 16 different sub-pixel locations for each sample mask position. This allows reaching a resolution determined by the size of the apertures in the sample mask [34], i.e., 12µm, in the x-direction, while resolution is driven by detector performance in the y-direction (approximately 100µm, sampled at 50µm) [30]. Features equal to or above this resolution will be detected in the attenuation and differential phase signals, whereas sub-resolution features appear in the dark-field signal [19]. The retrieval of attenuation, differential phase, and dark-field images is based on fitting Gaussian distributions on a pixel-by-pixel basis to the 19 images acquired at the different IC points with and without the sample, and comparing the resulting curves. In this specific case, a retrieval algorithm based on the three Gaussians fitting technique [35] was used to improve precision and minimize residual cross-talk effects from neighboring beamlets. Attenuation corresponds to the change in the Gaussian's amplitude, refraction (differential phase) to the shift of the Gaussian's center position, and dark-field to the broadening of the curve. For features equal to or above the resolution of the system, the standard deviation of the differential phase (STDP) was calculated for each ROI. It is sensitive to variations in the distribution of inhomogeneities on a scale larger than 12µm (since the system is only sensitive to phase effects in the x-direction, the resolution in y-direction is not relevant).

3. Results

First, the results from ultrasonic through-transmission signal absorption at 5 MHz were compared with the porosity values from the matrix digestion. Secondly, the three XPCi signals (attenuation, differential phase, and dark-field) were compared with the porosity values for the nine specimens, initially on a qualitative basis, and then quantitively. Finally, the STDP was introduced as a new method for measuring porosity in composite specimens and compared against the results of matrix digestion.

3.1 Ultrasonic attenuation

Ultrasonic through-transmission C-scans of the nine plate specimens were performed as detailed in section 2 to quantify variations in signal attenuation due to porosity. Figure 4 shows the C-scans for 4 representative plates covering the range of porosities available (10.7%, 6.6%, 3.9%, 0.7%). The bright yellow strips observed in the C-scan for the lowest porosity specimen are caused by the tape used to delimit the different ROIs (at 15 mm and 30 mm in Fig. 4(d)).

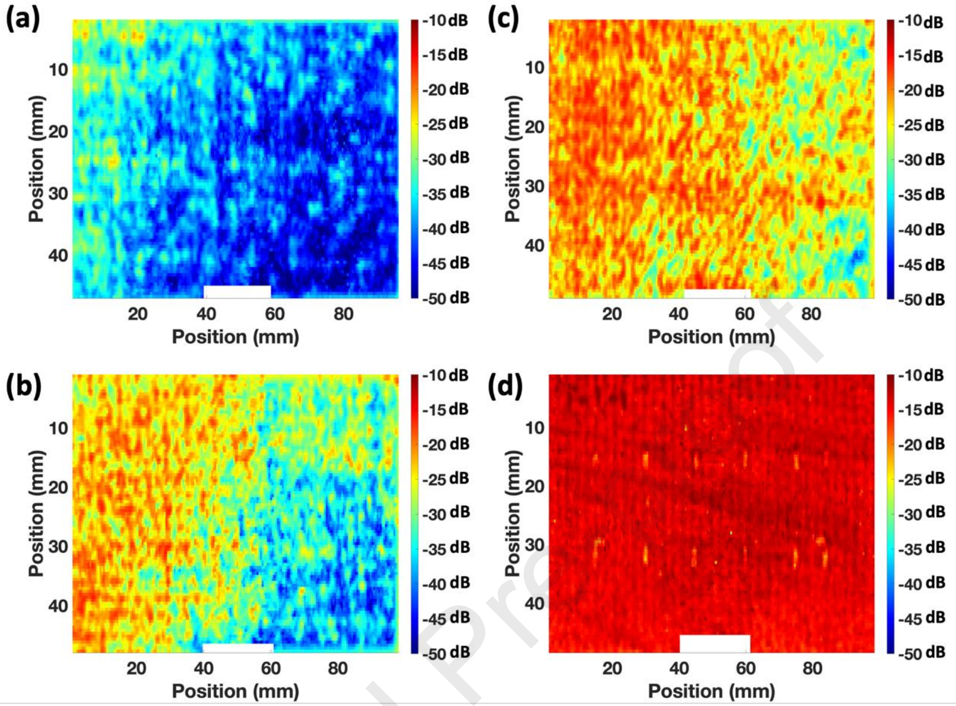

Figure 4: Ultrasonic signal attenuation (dB) C-scans of four plate specimens covering range of porosity: (a) 10.7%; (b) 6.6%; (c) 3.9%; (d) 0.7% nominal porosity. Areas of high attenuation (blue) correspond to increased porosity.

For the three higher porosity specimens, high and non-uniform ultrasonic attenuation was observed. For the specimen with the highest porosity (10.7%, Fig. 4(a)), a wide attenuation range of 35dB was measured across the plate, with the largest attenuation observed at the bottom right corner (blue color, corresponding to high porosity), and an average attenuation of -39±4dB (uncertainty corresponding to standard deviation, calculated over the scanned area). Even higher relative variation was observed for the 6.6% porosity plate (Fig. 4(b)), with -28±6dB attenuation. A lower average attenuation and variability of -23±1dB were measured for the 3.9% porosity plate (Fig. 4(c)). The areas of highest attenuation seem to be localized in the bottom right corner (blue color), which corresponds to the center of the large, manufactured panels, with lower attenuation observed on the left-hand side of the specimen. For the lowest porosity plate (0.7%, Fig. 4(d)), low and uniform ultrasonic signal attenuation with an average value of -14±1dB was observed.

The average ultrasonic attenuation and standard deviation for the nine plates is plotted against the porosity values obtained from matrix digestion in Fig. 5. The error bars for the porosity values from the destructive matrix digestion correspond to the standard error from the three small panels used, and not the accuracy stated in literature as approximately 0.5 percentage points [5, 7]. A strong correlation can be observed between the ultrasonic attenuation measurements and the porosity values obtained from matrix digestion, with an R^2 of 0.95. Ultrasonic attenuation increases approximately linearly with increasing porosity, as expected. However, for porosities below 2%, the ultrasonic measurements do not correlate well to the matrix digestion values, e.g., higher ultrasonic attenuation (-14±1dB) was measured for the lowest porosity plate (0.7%) than for the specimen with 1.5% porosity, which has the lowest ultrasonic attenuation signal (-9.2±0.2dB). Partially, the limited correlation could be due to the accuracy of matrix digestion making it difficult to resolve small differences between specimens with low porosity.

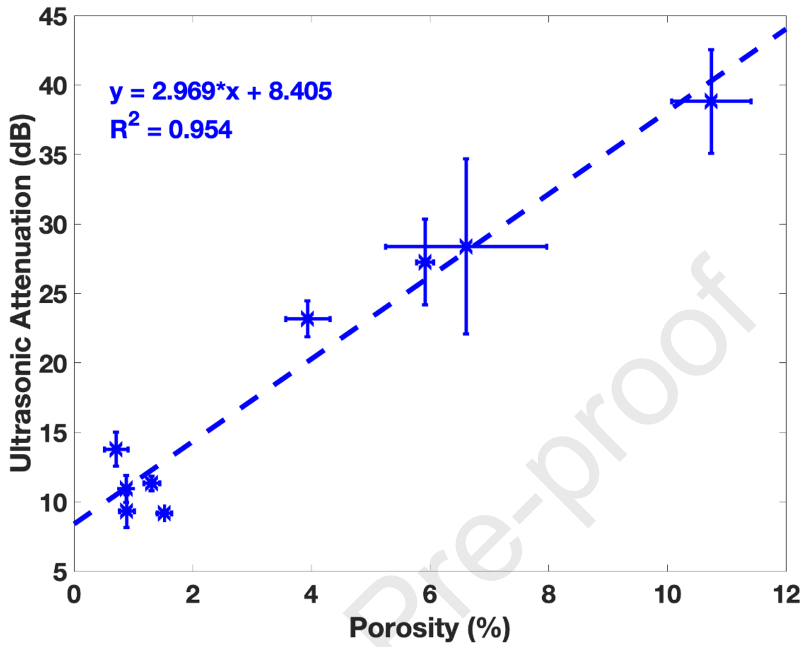

Figure 5: Average and standard deviation of ultrasonic attenuation for 9 plate specimens plotted against the porosity values obtained from matrix digestion.

3.2 XPCi measurements

3.2.1 Qualitative comparison of retrieved signals

The XPCi system can resolve inhomogeneities with a resolution of 12μm in the (one-directional) differential phase signal, and is sensitive to smaller (sub-micron) features through the dark-field signal [34]. The attenuation, differential phase, and dark-field signals were retrieved for the nine plates. Fig. 6 shows the three signals for a ROI extracted from the same plates with varying degrees of porosity shown in Fig. 4.

The one-dimensional phase sensitivity of the system makes the differential phase images directional, i.e., only features in the vertical direction in Fig. 6 are detected. The differential phase signal shows the edges of the inhomogeneities present in the samples, as these cause X-ray refraction at their interfaces. The attenuation and differential phase images show that the shape and structure of the inhomogeneities change between specimens with different levels of porosities. For the highest porosity plate (10.7%), and partly for the second highest (6.6%), the observed features seem to follow the woven pattern, with strong vertical features visible across the ROIs. Features become more irregular in the latter plate, suggesting a reduced clustering of the porosity around the fiber yarns. This is even more pronounced in the 3.9% porosity plate. Almost no irregular features are observed in the lowest (0.7%) porosity plate, with the aligned vertical features observed in the (direction of sensitivity of the) differential phase image thought to be due to the woven fiber yarn structures in the cross-ply plate.

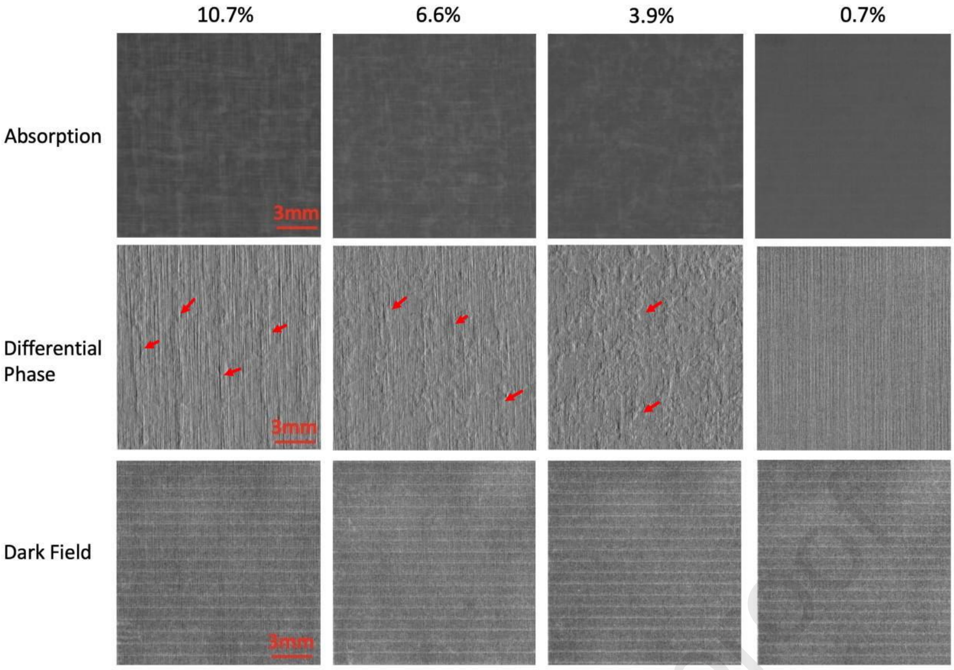

Figure 6: Attenuation (top), differential phase (middle), and dark-field (bottom) images of ROIs extracted from four plate specimens covering the considered range of porosities (left to right: 10.7%, 6.6%, 3.9%, and 0.7%). Arrows in the differential phase images indicate areas of high porosity.

No obvious features are discernible in the absorption and dark-field images, as the absorption signal has an inherent lack of sensitivity to small pores. As highlighted previously [23, 24], features in the dark-field images would arise from local variations in the distribution of inhomogeneities on the sub-resolution (i.e., <12 µm) scale. The lack of contrast variation in these images, alongside the clear visualization of structural inhomogeneities in the differential phase images (features >12µm resolved), suggests a lack of inhomogeneously distributed features on a scale below 12µm. This does not imply an absence of such microscopic features, and indeed a degree of correlation between dark-field signal and overall porosity level has been observed and is discussed below; only that they do not seem to cluster at specific locations. The horizontal lines visible in the dark-field images, as well as the brighter areas visible in the four corners of all images, are artefacts caused by interruptions in the mask apertures (see section 2).

3.2.2 Quantitative Comparison of EI-XPCi signals

Despite some features that can be attributed to porosity being visible in the attenuation images for the higher porosity plates (Fig. 6), very limited correlation was found between the average attenuation signal and the porosity values from the matrix digestion. As expected, no correlation was observed between the differential phase signals averaged over the scanned plate areas and the porosity values from the matrix digestion, since differential phase images highlight the edges of inhomogeneities with dark and bright fringes, which cancel out when averaged.

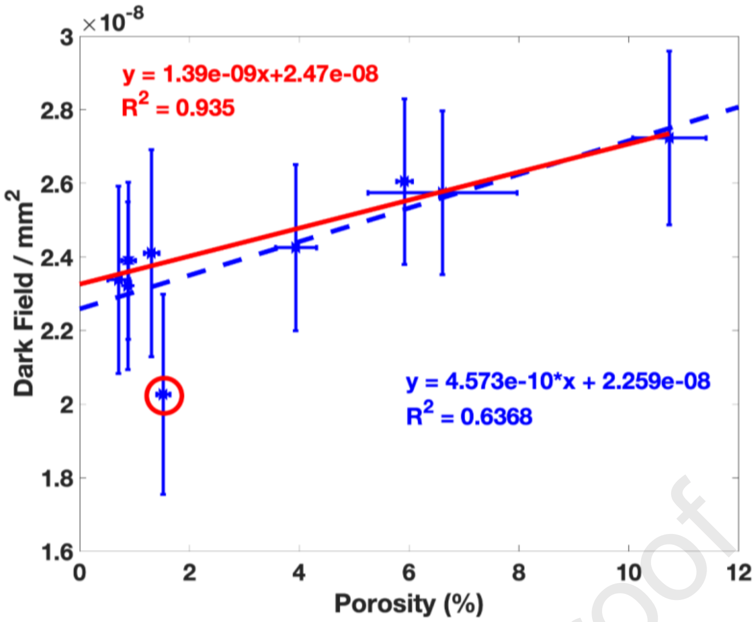

Figure 7: Average dark-field signal compared with the porosity values from matrix digestion for 9 specimens; linear fit for all specimens (blue, dashed), and improved fit obtained by eliminating the outlier in the red circle (red, solid).

Figure 7 shows the average dark-field signal plotted against the matrix digestion porosity values. Although no clear variation in inhomogeneity was observed in individual dark-field images (Fig. 6), correlation is observed between the averaged dark-field signals and porosity. Such correlation was previously observed for the presence of micro-cracks in CFRP, where the presence of features in the dark-field increased with increasing overall damage in the samples [17]. This supports the hypothesis that the dark-field signal is sensitive to sub-resolution features, and that their prevalence increases with increasing porosity levels. However, these appear to be uniformly distributed across the plates, leading to a variation in the overall value but not to observable local changes. The linear fit applied to all nine values has an R^2 value of 0.64 due to an outlier (circled in red). This outlier corresponds to the plate that was manufactured differently (section 2). The R^2 value increases to 0.94 when this plate is not considered, which is comparable to the results obtained with ultrasonic attenuation (0.95, see Fig. 5). However, it can be observed that, for plates below 4% porosity, the correlation is weak. This could indicate either that the number of sub-resolution features for the low porosity plates is similar, or that the sensitivity limits of the technique have been reached. Most importantly, the differential phase images in Fig. 6 clearly show the presence of inhomogeneities well above the resolution level, to which the dark-field signal is not sensitive.

3.2.3 Standard deviation of the differential phase

To take the above point into account, the analysis was extended by considering an additional approach, the standard deviation of the differential phase (STDP). This is sensitive to how many “edges” of features (on a scale above the resolution limit, i.e., >12µm) are detected per unit area, similar to the signal dark-field for inhomogeneities below the resolution limit. The STDP was calculated for each ROI, to ensure that a large enough area was covered. Images of the standard deviation of the differential phase for the same ROIs as in Fig. 6 are shown in Fig. 8. The images were produced by calculating the STDP over an area of 300µm by 300µm, thus extracting the signal over an area comparable to the ultrasonic resolution.

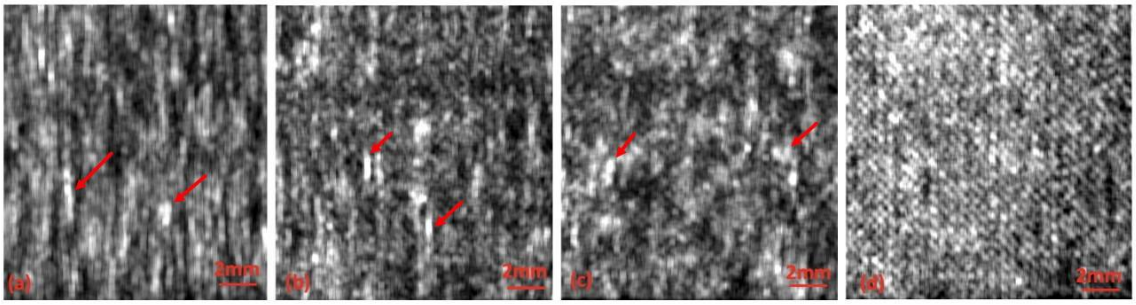

Figure 8: Comparison of the standard deviation of the differential phase (STDP) calculated over areas comparable to the resolution of the ultrasonic images (300μm by 300μm) for four plate specimens covering range of porosities: (a) 10.7%; (b) 6.6%; (c) 3.9%; (d) 0.7%. Arrows in panels (a-c) indicate areas of high porosity.

Areas with relatively high STDP correspond to large variations in the sample inhomogeneity on a scale equal to or larger than 12μm and are show as bright areas in Fig. 8. The contrast was adjusted independently for each image. In the highest porosity plate (10.7%), as expected, a feature distribution similar to the differential phase images is observed along the woven fiber yarns (see arrows in panel (a)), with bright vertical lines visible across the sample (due to the 1D sensitivity of the system). While the differential phase images highlight the edges of the porous regions, the STDP corresponds to their local distribution, with a high value effectively indicating “more features”. In the 6.6% porosity plate, the vertical porosity features are also visible but with lower intensity (see arrows in panel (b)), with additional high porosity areas distributed across the plate. For the 3.9% plate, the porosity is not aligned along the woven structure, and randomly distributed high intensity areas are visible across the ROI (examples indicated by arrows in panel (c)). A possible explanation might be that the reduction in porosity corresponds to a significantly decreased incidence of pores and defects aligned along the woven fiber yarns, but this would need further verification. In the image of the lowest porosity plate, the contrast has been stretched to an extent where some degree of the sample structure becomes visible; however, a gradient is also visible, indicating that more pores are present in the top/left area of the ROI compared to the bottom/right part.

The average STDP was calculated over the whole area of each ROI and integrated over the entire plate. This was plotted against the porosity obtained from the matrix digestion, as shown in Fig. 9. A strong correlation can be observed between STDP and the matrix digestion porosity values, demonstrating that STDP is capable of quantifying the degree of porosity in the plates. The R^2 value of 0.99 for the correlation between the standard deviation of the differential phase with the matrix digestion porosity values is the highest observed across all techniques, indicating even better correspondence than ultrasonic signal attenuation. Similarly, Kastner et al [7] found better correlation of porosity values obtained using nondestructive X-ray CT with matrix (acid) digestion than compared to ultrasonic testing, even though they state the same accuracy for matrix digestion and ultrasonic testing. For the low porosity plates (below 2%), the STDP increases with increasing matrix digestion porosity, showing better correlation than both the ultrasonic attenuation and the dark-field signal. STDP was capable of quantifying porosity content in the investigated woven composite plates down to low porosity values (<1%), whereas our ultrasonic attenuation measurements could not differentiate well between porosity values below 2%. These results correspond to a single sample orientation, resulting in sensitivity in a single direction.

However, STDP provides an estimate of the number of interfaces, expected to be approximately the same regardless of orientation, due to the continuous nature of the voids. It should be noted that the STDP signal intensity does not provide specific information on pore shape or size required for detailed stress analysis but enables rapid determination of the overall amount of porosity.

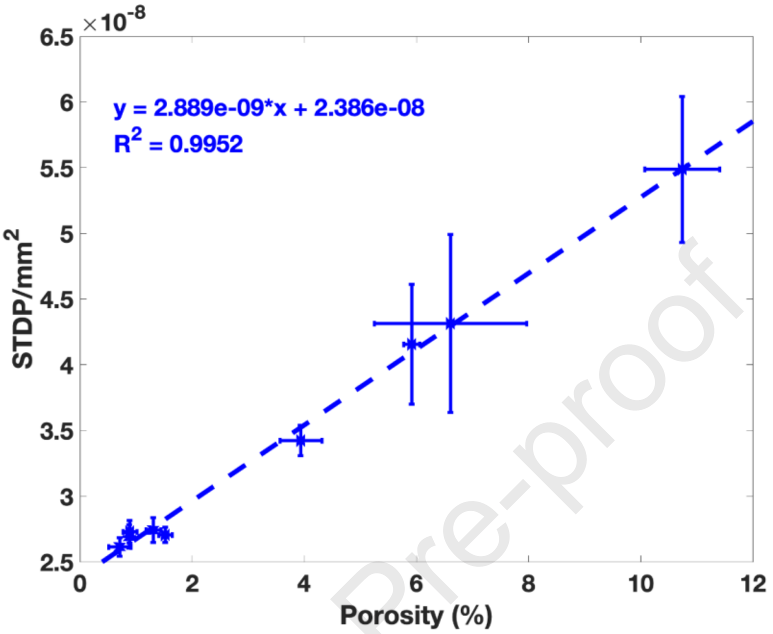

Figure 9: Comparison of average STDP with matrix digestion porosity values for all nine specimens.

4. Conclusions

Planar EI-XPCi was used for the quantification of porosity in fiber reinforced woven composite specimens, by comparing the retrieved signals to porosity content based on matrix digestion and ultrasonic attenuation measurements. Correlation was found between the porosity content calculated using matrix digestion and the dark-field signal, which is sensitive to inhomogeneities in the sub-resolution scale of the XPCi system (<12 μm). It was found that, for the set of specimens used in this investigation, the dark-field signal did not lead to a better correlation with matrix digestion porosity values than ultrasonic attenuation, possibly because of the relatively large pore size. The STDP (standard deviation of the differential phase) was therefore introduced, as a means to measure the variation in the distribution of inhomogeneity for features on a scale equal to or above the system resolution. The STDP was shown to have a better correlation than ultrasonic attenuation when compared with porosity values from matrix digestion, including for low porosity specimens (<2%), where ultrasonic attenuation and dark-field signals showed the least correlation. With the caveat that only the amount of porosity and not pore shape and size can be determined, and that some degree of calibration may be required, these results indicate significant potential for this new approach in the non-destructive evaluation of porosity content for fiber-reinforced composite specimens. In particular, STDP values can be extracted from relatively fast scans of large plate specimens [21] using planar (2D) imaging, which is faster and less restrictive on specimen size than X-ray micro-CT. However, it should also be noted that X-ray micro-CT can provide information on the spatial distribution in 3D, size, and shape of pores [7], which the proposed method cannot offer. Future work should include the investigation of the relation between STDP and dark-field signals. Scans with varying levels of system resolution (using masks with different aperture size) may allow effective means to combine the two signals, and offer the possibility to characterize pore and void size distribution on multiple scales through a single scan.

Declaration of interest:

DB is a Nikon employee. ME and AO are named inventors on UCL-owned patents protecting the EI-XPCI technology used to obtain the results presented in this paper. All other authors have no conflicts of interest to disclose.

Data Availability Statement

The raw/processed data required to reproduce these findings will be made available by the corresponding author upon request.

Funding: This work was supported by the UK Engineering and Physical Sciences Research Council (EPSRC) [grant numbers EP/N509577/1 and EP/T005408/1]. M. Endrizzi was supported by the Royal Academy of Engineering under their Eng. Research Fellowship scheme. A. Olivo was supported by the Royal Academy of Engineering under their Chairs in Emerging Technologies scheme.

References

1. Donadon M V., Iannucci L, Falzon BG, Hodgkinson JM, de Almeida SFM. A progressive failure model for composite laminates subjected to low velocity impact damage. Comput Struct. 2008;86:1232–52.
2. Birt EA, Smith RA. A review of NDE methods for porosity measurement in fibre-reinforced polymer composites. Insight. 2004;46(11):681–6.
3. Fernlund G, Wells J, Fahrang L, Kay J, Poursartip A. Causes and remedies for porosity in composite manufacturing. IOP Conf Ser Mater Sci Eng. 2016;139(1).
4. Mehdikhani M, Gorbatikh L, Verpoest I, Lomov S V. Voids in fiber-reinforced polymer composites: A review on their formation, characteristics, and effects on mechanical performance. J Compos Mater. 2019;53(12):1579–669.
5. Elkolali M, Nogueira LP, Rønning PO, Alcocer A. Void Content Determination of Carbon Fiber Reinforced Polymers: A Comparison between Destructive and Non-Destructive Methods. Polymers 2022, 14:1212.
6. EN 2564:2018. Aerospace series - Carbon fibre laminates - Determination of the fibre, resin and void contents (2018).
7. Kastner J, Plank B, Salaberger D, Sekelja J. Defect and porosity determination of fibre reinforced polymers by X-ray computed tomography. NDT in Aerospace 2010
8. Yang P, Elhajjar R. Porosity Content Evaluation in Carbon-Fiber/Epoxy Composites Using X-ray Computed Tomography. Polym - Plast Technol Eng. 2014;53(3):217–22.
9. Wildenschild D, Sheppard AP. X-ray imaging and analysis techniques for quantifying pore-scale structure and processes in subsurface porous medium systems. Adv Water Resour. 2013;51:217–46.
10. Guo N, Cawley P. The non-destructive assessment of porosity in composite repairs. Composites. 1994;25(9):842–50.
11. Daniel IM, Wooh SC, Komsky I. Quantitative porosity characterization of composite materials by means of ultrasonic attenuation measurements. J Nondestruct Eval. 1992;11(1):1–8.
12. Smith RA, Nelson LJ, Mienczakowski MJ, Wilcox PD. Ultrasonic Analytic-Signal Responses from Polymer-Matrix Composite Laminates. IEEE Trans Ultrason Ferroelectr Freq Control. 2018;65(2):231–43.
13. van Dreumel WHM. Ultrasonic scanning for quality control of advanced fibre composites, NDT Int. 1978;11(5):233-5.
14. Manta A, Gresil, M, Soutis, C. Infrared thermography for void mapping of a graphene/epoxy composite and its full-field thermal simulation, Fatigue Fract Eng Mater Struct. 2019;42:1441–1453.
15. Fitzgerald R. Phase-Sensitive X-Ray Imaging. Phys Today. 2000;53:23–6.
16. Olivo A, Castelli E. X-Ray Phase Contrast Imaging: From Synchrotrons to Conventional Sources. Riv del Nuovo Cim. 2014;37(9):467–508.
17. Senck S, Scheerer M, Revol V, Plank B, Hannesschläger C, Gusenbauer C, et al. Microcrack characterization in loaded CFRP laminates using quantitative two- and three-dimensional X-ray dark-field imaging. Compos Part A Appl Sci Manuf. 2018 Dec;115:206–14.
18. Coindreau O, Vignoles G, Goyheneche J-M. Multiscale X-Ray CMT of C/C Composite Preforms: A Tool for Properties Assessment. In: Ceramic Transactions, Advances in Ceramic Matrix Composites. Hoboken, NJ, USA: John Wiley & Sons, Inc.; 2006. p. 77–84.

19. Endrizzi M, Diemoz PC, Millard TP, Louise Jones J, Speller RD, Robinson IK, et al. Hard X-Ray Dark-Field Imaging with Incoherent Sample Illumination. Appl Phys Lett. 2014;104(2):3–6.
20. Endrizzi M, Diemoz PC, Hagen CK, Millard TP, Vittoria FA, Wagner UH, et al. Laboratory-based Edge-illumination Phase-contrast Imaging : Dark-field Retrieval and High-resolution Implementations. In: 2014 IEEE Nuclear Science Symposium and Medical Imaging Conference (NSS/MIC). 2012. p. 1–3.
21. Astolfo A, Endrizzi M, Vittoria FA, Diemoz PC, Price B, Haig I, et al. Large field of view, fast and low dose multimodal phase-contrast imaging at high x-ray energy. Sci Rep. 2017;7(1):1–8.
22. Diemoz PC, Hagen CK, Endrizzi M, Olivo A. Sensitivity of laboratory based implementations of edge illumination X-ray phase-contrast imaging. Appl Phys Lett. 2013;103(24).
23. Shoukroun D, Massimi L, Iacoviello F, Endrizzi M, Bate D, Olivo A, et al. Enhanced composite plate impact damage detection and characterisation using X-Ray refraction and scattering contrast combined with ultrasonic imaging. Compos Part B. 2020;181(107579):1–10.
24. Endrizzi M, Murat BIS, Fromme P, Olivo A. Edge-illumination X-Ray Dark-Field Imaging for Visualising Defects in Composite Structures. Compos Struct. 2015;134(1):895–9.
25. Revol V, Jerjen I, Kottler C, Schtz P, Kaufmann R, Lthi T, et al. Sub-pixel porosity revealed by x-ray scatter dark field imaging. J Appl Phys. 2011;110(4):1–6.
26. Gusenbauer C, Reiter M, Plank B, Salaberger D, Senck S, Kastner J. Porosity Determination of Carbon and Glass Fibre Reinforced Polymers Using Phase-Contrast Imaging. J Nondestruct Eval. 2019;38(1):1–10.
27. HexPly ® M21 180C Curing Epoxy Matrix Report. 2020.
28. ASTM D3171-15. In: Standard Test Methods for Constituent Content of Composite Materials. West Conshohocken, PA: ASTM International; 2015.
29. Stone DEW, Clarke B. Ultrasonic attenuation as a measure of void content in carbon-fibre reinforced plastics. Non-Destructive Test. 1975;8(3):137–45.
30. Massimi L, Suaris T, Hagen CK, Endrizzi M, Munro PRT, Havariyoun G, et al. Detection of involved margins in breast specimens with X-ray phase-contrast computed tomography. Sci Rep. 2021;11(3663):1–9.
31. Olivo A, Ignatyev K, Munro PRT, Speller RD. Design and realization of a coded-aperture based x-ray phase contrast imaging for homeland security applications. Nucl. Instrum. Meth. Phys. Res. A 2009;610:604-14
32. Millard TP, Endrizzi M, Ignatyev K, Hagen CK, Munro PRT, Speller RD, et al. Method for automatization of the alignment of a laboratory based x-ray phase contrast edge illumination system. Rev Sci Instrum. 2013;84(8).
33. Ignatyev K, Munro PRT, Speller RD, Olivo A. Effects of signal diffusion on x-ray phase contrast images. Rev Sci Instrum. 2011;82(073702):1–9.
34. Diemoz PC, Vittoria FA, Olivo A. Spatial resolution of edge illumination X-ray phase-contrast imaging. Opt Express. 2014;22(13):15514.
35. Maughan Jones CJ, Vittoria FA, Olivo A, Endrizzi M, Munro PRT. Retrieval of weak x-ray scattering using edge illumination. Opt Lett. 2018;43(16):3874.

15th December 2021
Re: Author Contributions

The Contributor Roles Taxonomy for the manuscript "Quantification of Porosity in Composite Plates using Planar X-ray Phase Contrast Imaging" are:

Dana Shoukroun: Methodology, Formal Analysis, Validation, Investigation, Data Curation, Writing – Original Draft, Visualization; **Lorenzo Massimi**: Methodology, Writing – Review & Editing; **Marco Endrizzi**: Methodology, Writing – Review & Editing; **Alan Nesbitt**: Resources, Data Curation, Writing – Review & Editing; **David Bate:** Resources, Writing – Review & Editing, Funding Acquisition; **Paul Fromme**: Conceptualization, Validation, Resources, Writing – Review & Editing, Supervision; **Alessandro Olivo**: Conceptualization, Methodology, Validation, Resources, Writing – Review & Editing, Supervision, Funding Acquisition.

Yours sincerely,
Dana Shoukroun

Declaration of interests

☐ The authors declare that they have no known competing financial interests or personal relationships that could have appeared to influence the work reported in this paper.

☒The authors declare the following financial interests/personal relationships which may be considered as potential competing interests:

DB is a Nikon employee. ME and AO are named inventors on UCL-owned patents protecting the EI-XPCI technology used to obtain the results presented in this paper. All other authors have no conflicts of interest to disclose.